Structural basis of gene regulation by the tetracycline inducible Tet repressor–operator system

Peter Orth[1], Dirk Schnappinger[2], Wolfgang Hillen[2], Wolfram Saenger[1] and Winfried Hinrichs[1,3]

[1]Institut für Chemie, Kristallographie, Freie Universität Berlin, Takustr. 6, D-14195 Berlin, Germany. [2]Institut für Mikrobiologie und Biochemie, Friedrich-Alexander Universität Erlangen, Staudtstr. 5, D-91058 Erlangen, Germany. [3]Institut für Chemie und Biochemie, Ernst-Moritz-Arndt Universität Greifswald, Soldmannstr. 16, D-17487 Greifswald, Germany.

The tetracycline repressor (TetR) regulates the most abundant resistance mechanism against the antibiotic tetracycline in gram-negative bacteria. The TetR protein and its mutants are commonly used as control elements to regulate gene expression in higher eukaryotes. We present the crystal structure of the TetR homodimer in complex with its palindromic DNA operator at 2.5 Å resolution. Comparison to the structure of TetR in complex with the inducer tetracycline-Mg^{2+} allows the mechanism of induction to be deduced. Inducer binding in the repressor core initiates conformational changes starting with C-terminal unwinding and shifting of the short helix α6 in each monomer. This forces a pendulum-like motion of helix α4, which increases the separation of the attached DNA binding domains by 3 Å, abolishing the affinity of TetR for its operator DNA.

In gram-negative bacteria, resistance to the antibiotic tetracycline (Tc; Fig. 1) most commonly results from export of the tetracycline-magnesium complex, $[MgTc]^+$, by the TetA protein, which is embedded in the cytoplasmic membrane[1,2]. Expression of TetA is under tight transcriptional control of the tetracycline repressor (TetR)[3,4]. Binding of $[MgTc]^+$ to TetR abolishes DNA binding to two palindromic operator sites (*tetO*1,2) and thus allows transcription of the divergently oriented genes *tetR* and *tetA*[5]. High level expression of TetA is lethal for the bacterial cell because nonspecific cation transport causes the cytoplasmic membrane potential to collapse[6]. This requires a well-defined repressed status of the *tetA* gene by strong binding of TetR to *tetO* (association constant $K_a \sim 10^{11}\ M^{-1}$). Tc binds to ribosomes ($K_a \sim 10^6\ M^{-1}$), inhibiting protein synthesis, and thus TetR is required to be a particularly sensitive switch. Binding of $[MgTc]^+$ to TetR ($K_a \sim 10^9\ M^{-1}$) reduces the affinity of TetR for *tetO* by nine orders of magnitude[7,8]. This guarantees that the silent (TetR bound to *tetO*) and the active (TetR bound to $[MgTc]^+$) states of *tetO* are efficiently discriminated and subinhibitory Tc concentrations are sufficient to allow transcription to proceed. Since TetR–*tetO* is the most efficiently inducible system of transcriptional regulation known so far, it is commonly used as a tool for selective target-gene regulation in eukaryotes[9–13].

Here, we present the crystal structure of TetR in complex with a palindromic, 15 base pair *tetO* fragment at 2.5 Å resolution. Crystal structures are now available for all biologically relevant TetR states, the TetR–$[MgTc]^+$ complex[14,15], and the free TetR[16]. This allows detailed examination of the molecular mechanisms underlying the control of TetR–operator complex formation and dissociation, which differ from those of comparable transcription regulators such as Trp repressor[17] or Lac repressor[18] and purine repressor[19] of the LacI/GalR family.

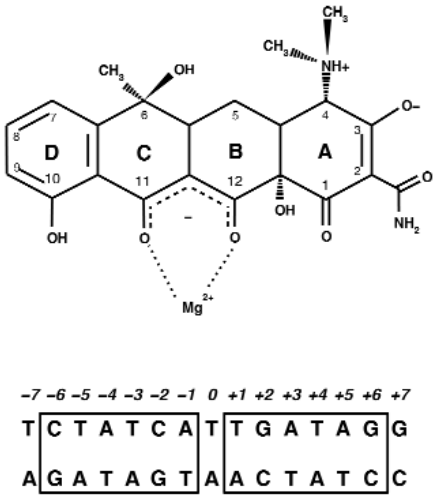

Fig. 1 ***a***, Chemical structure of the tetracycline-Mg^{2+} complex occurring under physiological conditions. ***b***, Sequence of the 15 base pair *tet*-operator used for co-crystallization. The boxes refer to the palindromic symmetry of *tetO*.

All of the crystallographic results reported here are based on TetR of the resistance determinant class D, which shares about two thirds sequence identity with the extensively characterized TetR of class B[4]. The oligonucleotide sequences of the corresponding *tetO1* sites only differ by one base pair. Consequently, we can assume that the discussed sequence specific interactions of TetR with *tetO1* or $[MgTc]^+$ will be nearly identical between the two classes.

Architecture of TetR

Each polypeptide chain (residues 2–208) of the functional TetR homodimer is folded into 10 α-helices (α1–α10 and α1'–α10', respectively; Fig. 2). Two small, N-terminal, DNA-binding

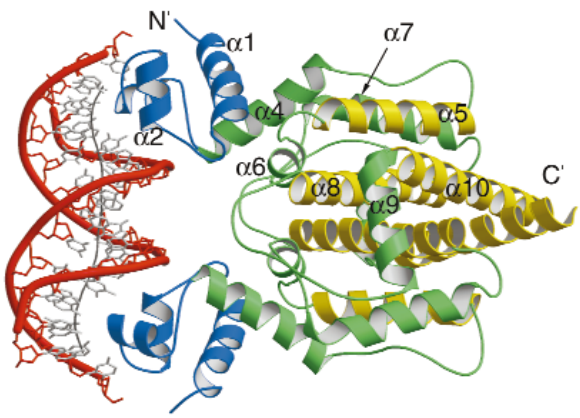

Fig. 2 Structure of the TetR–*tetO* complex. The α-helices of the homodimeric TetR are labeled in one monomer (dyad axis horizontal). The DNA-binding domains (helices α1 to α3) are blue, helices of the rigid scaffold (α5, α8, α10) are yellow and helices undergoing conformational changes upon induction (α4, α6, α9 and to some extent α7) are green. The curvature of the 15 base pair operator fragment is represented by a gray line (calculated with CURVES[41]), the phosphate-ribose backbone is in red and bases in gray. The central third of the *tetO* fragment is straight, the curvature of each half operator is caused by TetR binding to the major groove. Figures were drawn using MOLSCRIPT[42] and RASTER3D[43].

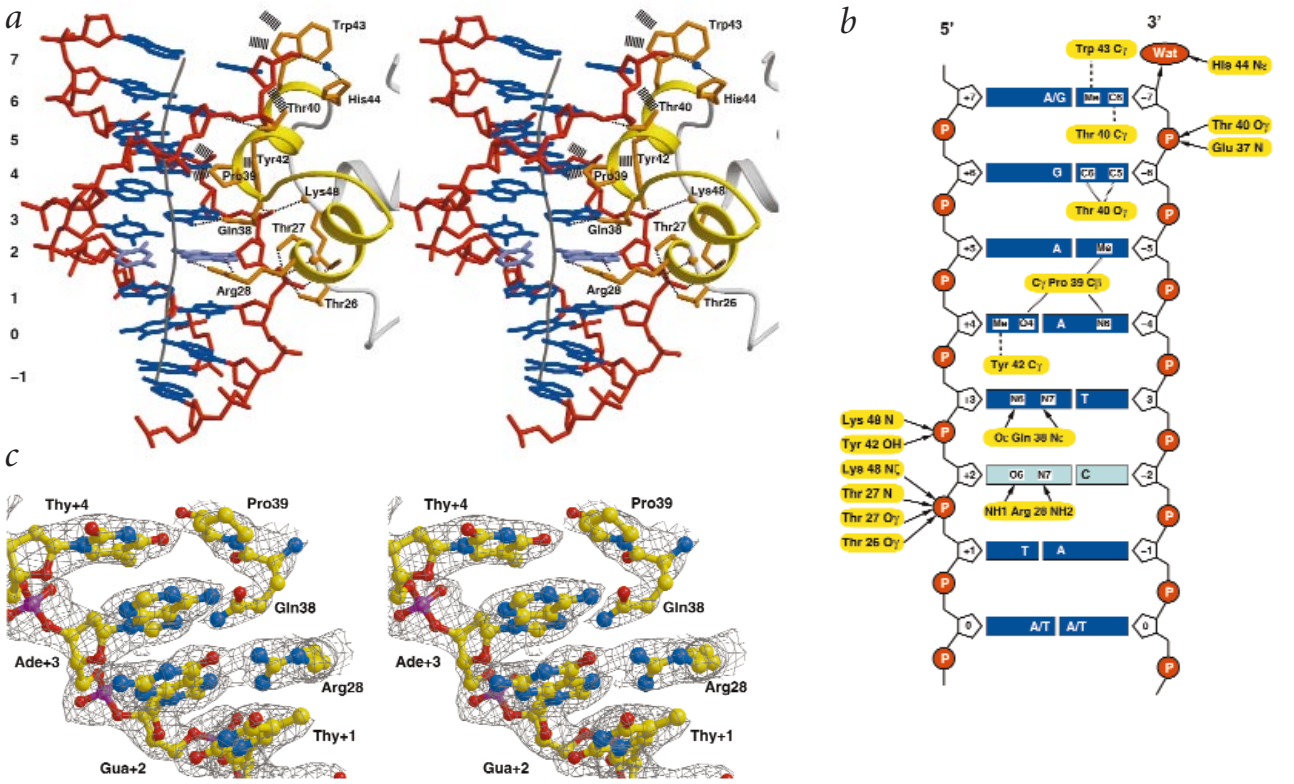

Fig. 3 Sequence specific TetR–*tetO* interactions. ***a***, Stereo view of one DNA-binding domain (α1 to α3) and the corresponding half-operator (base pairs 0 to 7, phosphate-ribose backbone in red and bases in blue, the kink at base pair 2 in purple). HTH-motif (residues 27–44) in yellow, other parts of TetR in white. The N-terminus of helix α4 (white) is at Lys 48, linking the DNA-binding domain to the regulatory domain. Amino acid side chains contacting the operator DNA are labeled and hydrogen bonds are indicated by thin broken lines, hydrophobic contacts are indicated by thick broken lines. The DNA curvature is presented by a gray line. ***b***, Schematic representation of interactions between TetR and the 15 base pair operator. The color scheme is the same as in (*a*). Hydrogen bonds are shown as arrows, van der Waals interactions (≤3.5 Å) by dotted lines. A water molecule is located at the phosphate position connecting base pairs 7 and 8 in *tetO*, and mimics a direct His 44Nε···O–P hydrogen bond. The side chain of Pro 39 switches TetR binding from one *tetO* strand to the other at T4 to T-5. ***c***, Representative electron density of the central part of (*a*) showing the specific interactions G2, A3 and T4 with Arg 28, Gln 38 and Pro 39, respectively.

domains are formed by three-helix bundles (α1–α3) within which α2 and α3 (residues 27–44) constitute classical helix-turn-helix (HTH) motifs[20]. Regulation of TetR by binding of $[MgTc]^+$ takes place in the core of the TetR homodimer, which is formed by helices α5 to α10 and α5' to α10'. The N-terminal part of helix α4 (residues 48–63) contributes to the hydrophobic center of the DNA-binding domain and links it to the regulatory domain of TetR. The central part of the regulatory domain consists of the anti-parallel helices α8, α10 and the dyad-related α8', α10'. Superposition of the structures of TetR in complex with either $[MgTc]^+$ or *tetO* reveals that this four-helix bundle, together with α5, α5', form the rigid scaffold for two equivalent, tunnel-like, inducer binding pockets.

DNA structure and TetR recognition

The crystallographic results reveal additional features of the sequence specific TetR–*tetO* interactions proposed by genetic and biochemical studies[21–25]. In the DNA-bound complex, the two-fold symmetry of TetR is maintained (Fig. 2). Each HTH-motif binds to the corresponding major groove of the palindromic operator, whereas the minor groove is not recognized by TetR. All base pairs of the 15-mer operator fragment, except the central three pairs, are engaged in TetR binding (Fig. 3). The central base pair (designated base pair 0) is required as a spacer for the half-operators and does not contribute to sequence specificity.

In contrast to the well accepted role of water molecules for both the specificity and affinity of protein–DNA interactions[26], no water molecules are incorporated into the protein–DNA interface. Therefore, we can assume a high entropy term for the binding constant of TetR to *tetO* caused by release of water at the TetR–*tetO* interface. There is no 'empty' space in the interface region that could be filled by disordered water molecules. Only one water molecule connects side chains of Thr 26 and Arg 28 (N-terminal to the HTH) and orients them for DNA-binding.

The N-terminus of the recognition helices α3, α3' point towards the palindromic center of *tetO* while the helix axes are aligned parallel to the major groove, each forming an angle of ~33 with respect to the axis of the DNA double helix (Fig. 2). At the recognition site, the major groove is widened to 14–14.5 Å (canonical B-DNA 11.7 Å), whereas at the central base pair, the major groove on the opposite side of the TetR interface is narrowed to 9.5 Å. These differences are associated with corresponding changes of the minor groove resulting in partial unwinding of the DNA duplex, which increases the helical repeat to 38 Å (B-DNA 34 Å). Each half-operator is kinked away from TetR at base pair 2, but the ends of the 15-mer *tetO* fragment are almost parallel to each other, because the kink is compensated along base paris 3–6 by bending towards the protein (Fig. 3).

The kink at position G2 is caused by several hydrogen bonds, which are formed between the phosphate groups attached to the

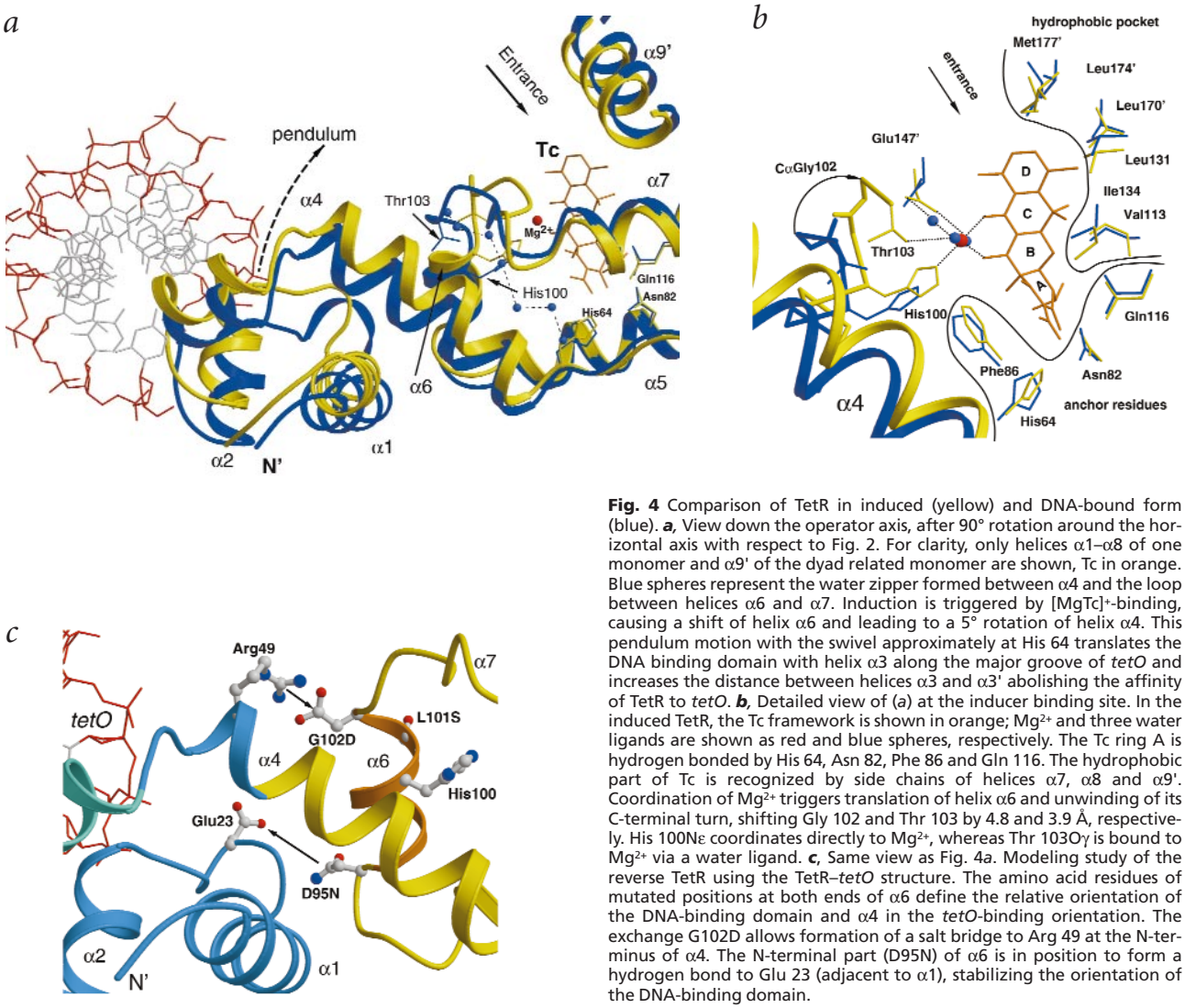

Fig. 4 Comparison of TetR in induced (yellow) and DNA-bound form (blue). ***a***, View down the operator axis, after 90° rotation around the horizontal axis with respect to Fig. 2. For clarity, only helices α1–α8 of one monomer and α9' of the dyad related monomer are shown, Tc in orange. Blue spheres represent the water zipper formed between α4 and the loop between helices α6 and α7. Induction is triggered by $[MgTc]^+$-binding, causing a shift of helix α6 and leading to a 5° rotation of helix α4. This pendulum motion with the swivel approximately at His 64 translates the DNA binding domain with helix α3 along the major groove of *tetO* and increases the distance between helices α3 and α3' abolishing the affinity of TetR to *tetO*. ***b***, Detailed view of (*a*) at the inducer binding site. In the induced TetR, the Tc framework is shown in orange; Mg^{2+} and three water ligands are shown as red and blue spheres, respectively. The Tc ring A is hydrogen bonded by His 64, Asn 82, Phe 86 and Gln 116. The hydrophobic part of Tc is recognized by side chains of helices α7, α8 and α9'. Coordination of Mg^{2+} triggers translation of helix α6 and unwinding of its C-terminal turn, shifting Gly 102 and Thr 103 by 4.8 and 3.9 Å, respectively. His 100Nε coordinates directly to Mg^{2+}, whereas Thr 103Oγ is bound to Mg^{2+} via a water ligand. ***c***, Same view as Fig. 4*a*. Modeling study of the reverse TetR using the TetR–*tetO* structure. The amino acid residues of mutated positions at both ends of α6 define the relative orientation of the DNA-binding domain and α4 in the *tetO*-binding orientation. The exchange G102D allows formation of a salt bridge to Arg 49 at the N-terminus of α4. The N-terminal part (D95N) of α6 is in position to form a hydrogen bond to Glu 23 (adjacent to α1), stabilizing the orientation of the DNA-binding domain.

3'- and 5'-positions of the ribose and amino acid side chains (Thr 26, Thr 27, Tyr 42 and Lys 48) and NH groups of the peptide main chain (Thr 27, Lys 48) (Fig. 3). In a comparable manner, the 3'- and 5'-phosphate groups of the anti-parallel operator strand of base pair -7 are also hydrogen bonded by main chain (Glu 37N of the HTH turn) and side chain contacts (Thr 40, His 44). In this way hydrogen bonds to phosphate groups cover each distorted half-operator recognized by TetR (Fig. 3*b*).

At the kink, the stacking distance between base pair 1 and 2 is increased to 3.9 Å (B-DNA 3.4 Å), stabilized by sequence specific hydrogen bonds between both purine bases G2 and A3 and the side chains of Arg 28 and Gln 38, respectively (Fig. 3*c*). In the bent half-operator, all residues of helix α3 contribute to sequence specific oligonucleotide recognition, except Leu 41, which is part of the hydrophobic core stabilizing the three-helix bundle. The recognition helix α3 (residues 38–44) is one to two turns shorter compared to other prokaryotic regulatory proteins[15,27]. Intensive operator interaction of α3 is indicated by N-terminal distortion to form a 3_{10}-helical turn. TetR–*tetO* interactions of this short α3 helix are supported by residues, which are not in the HTH sequence, but are sterically close to the binding motif (Fig. 3*a*). Hydrogen bonds are indicated between *tetO* phosphate groups and main chain peptide N H groups and side chains of amino acid residues (Thr 26, Lys 48). These properties suggest high structural complementary of *tetO* and the DNA-binding domains of TetR.

Inducer binding and signal transduction

The distance and relative orientation of the HTH motifs distinguish between the induced and non-induced status of TetR, because the center-to-center separation of the recognition helices α3, α3' in the operator complex increases upon inducer binding from 36.6 Å to 39.6 Å. As the $[MgTc]^+$-binding site is about 33 Å apart from the *tetO*-binding interface, a sequence of structural changes transfers the induction signal to the DNA-binding domain.

After $[MgTc]^+$-insertion into the binding tunnel, ring A of Tc is anchored by hydrogen bonds between its functional groups and the side chains of His 64 (C-terminus of α4), Asn 82, Phe 86 (both on α5) and Gln 116 (α7) (Fig. 4). These amino acids remain in position after inducer binding[16], but the Tc-chelated Mg^{2+}-ion displaces His 100 and Thr 103 of the short helix α6 (residues 96–102) by 1.9 and 3.9 Å, respectively.

This is facilitated by a shift of helix α6 in its C-terminal direction by 1.5 Å and a 'peeling off' of its C-terminal turn to form a type II β-turn (residues 100–103). These conformational changes initiate the induction process, as helix α6 (with residues Val 99, Thr 103) is in van der Waals contact with helix α4 (with residues Leu 52, Ala 56); these helices intersect at an angle of approximately -130°. The translation of α6 forces the central part of α4 to shift in the same direction. Because the C-terminus of α4 is fixed to the regulatory domain with His 64 anchored to Tc, the N-terminus swings in a pendulum-like motion by about 5° (Fig. 4). As a consequence of the rotations of α4 and α4', the respective N-terminal DNA-binding domains are shifted apart, increasing the separation of the recognition helices α3, α3' by 3 Å. The shift of the recognition helices along the major groove disrupts the contacts between the DNA-binding domain and the respective half-operator, causing dissociation of the TetR–*tetO* complex. All these events obey the constraint of the two-fold rotational symmetry inherent in the TetR homodimer.

The conformational change in α6 to form the β-turn requires displacement of all residues (up to 4.8 Å for residues 102–106) of the adjacent loop connection between helices α6 and α7. This allows formation of an extended network of cooperative hydrogen bonds including a chain of eight water molecules ('water zipper'), which fix the linker helix α4 after its reorientation[16] (Fig. 4).

The reverse Tet repressor

Using random mutagenesis, a mutant of the class B TetR was identified that shows increased, instead of decreased, affinity to *tetO* upon inducer/effector binding. This 'reverse TetR' is commonly used to regulate gene expression in higher eukaryotes[9]. The reverse phenotype depends on mutations that restrict the repressor to a non-inducible conformation (G102D, L101S) and on mutations that lock the DNA binding domains in the position necessary for operator binding (D95N, G102D).

Mutations at position Gly 102 are not inducible[28]. Any variation of this residue causes sterical hindrance and interferes directly with the formation of the β-turn next to α6 (ref. 16). This is supported by the L101S exchange which probably stabilizes the C-terminus of α6 preventing β-turn formation. Tc binding in the absence of β-turn formation does not induce TetR. This is evidenced by Mg^{2+}-free TetR–Tc complexes that are in the non-induced conformation despite being bound to Tc[29].

The substitutions D95N and G102D are located at both ends of α6 and are in conserved positions within all TetR classes (Fig. 4*c*). Both substitutions stabilize the orientation of the DNA-binding domain required for *tetO* binding. Asp 102 is in a position to form a salt bridge to Arg 49 at the N-terminus of α4, fixing the relative orientation of helices α4 and α6. The D95N mutation allows a hydrogen bond to Glu 23 in the C-terminus of α1.

The most potent effectors for the reverse TetR are Tc analogs that lack the hydroxyl group at position 6 (Figs 1,4*b*)[9]. Modifications at position 6 enhance Tc binding to the hydrophobic part of the binding tunnel and presumably stabilize the protein core[30,31] since Tc replaces several water molecules in the binding tunnel[16] and thus contributes to the etropy of the system.

Comparison of repressor systems

Most members of the highly homologous lactose repressor (LacI) family bind with high affinity to their operator DNA in absence of their regulating small ligand, whereas purine repressor (PurR) requires corepressor binding (guanine or hypoxanthine) for specific interaction to the operator[32,33]. An extreme situation for the reverse function of a ligand controlled repressor system is the reverse phenotype of TetR discussed above.

In addition to the structures of the TetR and complexes in the TetR system, structures of repressor–operator complexes and the apo repressors have been determined for PurR[19], the tryptophan repressor (TrpR)[19], and LacI[18]. As in case of TetR, these homodimeric repressors recognize their specific operator DNA sites using HTH motifs, and binding or release is regulated by small molecules.

Trp repressor binding to its specific operator sequence is initiated by the effector molecule L-tryptophan, which binds in pockets below the C-terminal HTH motifs. The tryptophan ligand reorients the mobile HTH motifs to fit into successive major grooves of operator DNA. The bound tryptophan molecules are part of the DNA recognition pattern since indols hydrogen bond to the DNA phosphate backbone[17]. In contrast, the effector binding sites in PurR, LacI and TetR are located far away from the protein–DNA interfaces, and thus direct interaction of the effector molecules with operator DNA is not possible.

PurR and LacI each have an N-terminal three-helix bundle, a hinge region for specific DNA binding and a bipartite core domain with two topologically similar subdomains. The rela-

Table 1 Summary of data collection and refinement statistics

Data collection[1]	
Resolution (Å)	24.5–2.5
Space group	Orthorhombic $C222_1$
Unit cell (Å)	a = 38.04, b = 193.2, c= 91.75
Measured / unique reflections	42,624 / 11,520 (Redundancy 3.7)
Completeness (%) (last shell)	97.2 (94.4)
I/σ(I) (last shell)[2]	12.1 (3.3)
R_{sym} (%)[3] (last shell)	9.0 (28.7)
Wilson B-factor (Å^2)	57.9
Refinement	
R-factor (%) / R_{Free}(%)[4]	24.4 / 30.7
Number of atoms	
TetR / *tetO* / water / imidazole	1,551 / 321 / 41 / 5
Average overall isotropic B-factors (Å^2)	
Protein main chain / side chain	44.6 / 47.5
Oligonucleotide	55.0
Water, imidazole	48.9
R.m.s. deviations from idealized geometry[5]	
Bond lengths (Å)	0.008
Bond angles (°)	1.34
Torsion angles (°)	20.6

[1]Source: rotating anode, type FR571, NONIUS GmbH 0.2 × 2 mm^2 focal spot size; 45kV, 65 mA. Wavelength: Cu Kα, Graphite monochromator. Detector: MarResearch image plate, 180 mm diameter. Temperature: cooling device 100 K, Oxford Cryosystems.
[2]I/σ(I) = ratio mean intensity to mean standard deviation.
[3]$R_{sym} = \Sigma \mid I - \langle I \rangle \mid / \Sigma I$, where I is the observed intensity and <I> the average intensity of multiple symmetry-related observations of that reflection.
[4]R-factor = $\Sigma \parallel F_{obs} \mid - \mid F_{calc} \parallel / \Sigma \mid F_{obs} \mid$ and R_{Free} is calculated from 10% of randomly chosen reflections, excluded from refinement for cross-validation.
[5]There were no Ramachandran outliers.

tive arrangement of the three helices in the DNA binding domain of PurR (HTH-loop-helix) is similar to that in TetR, but the order of the helices has changed to helix-loop-HTH. This situation might be termed a local jelly roll.

The bipartite core of PurR and LacI is the basis for the allosteric mechanism[32–34]. Transformation of the repressed to the induced state is caused by ligand binding at the interface of the two subunits in each monomer. The C-terminal subdomains remain fixed and conformational changes that occur are localized in the N-terminal subdomains. In contrast to TetR, they move and rotate against each other and propagate a structural change that affects DNA binding by the three-helix bundles and the hinge helices that undergo a coil-to-helix transition[18,19]. The short hinge helices (two turns) form an antiparallel pair and intercalate into the minor groove supporting the central distortion of the operator DNA, which is kinked away from the repressor. Other homodimeric repressor proteins with HTH motifs lacking these minor groove binding helices show an overall bending of DNA towards the protein.

Methods

Crystallization and data collection. TetR was co-crystallized with the 15 base pair *tet*-operator as reported[35]. X-ray diffraction data were collected from one single crystal using CuKα radiation. Crystals were flash-frozen in liquid propane and measured in a gaseous stream of nitrogen at 100 K. Data were reduced using the HKL package[36] and further processed with programs of the CCP4 suite[37].

Structure solution and refinement. The structure was solved by molecular replacement with the program AMoRe[38] using the polypeptide chain of TetR–$[MgTc]^+$ (PDB accession code 2TCT) as search model. The correct solution corresponded to the top peaks in both the rotation and translation function. After rigid-body refinement phasing was sufficient for model building of the *tetO* fragment, using the program O[39]. Refinement was assisted by molecular dynamics using X-PLOR[40]. The dimeric TetR–*tetO* complex is located on a crystallographic dyad and the asymmetric unit of the model consists of a TetR monomer (residues 4–155 and 164–206) and 15 nucleotides of a DNA single strand. Statistics are given in Table 1.

Coordinates. Atomic coordinates have been deposited in the Protein Data Bank (accession code 1QPI).

Acknowledgments

Helpful discussions with A. Steinmetz and T. Simonson (IGBMC, Strasbourg) and DNA purification and cocrystallization by C. Alings are gratefully acknowledged.

This work was supported by grants of the Deutsche Forschungsgemeinschaft (Sonderforschungsbereich 344) and by Fonds der Chemischen Industrie.

Correspondence should be addressed to W.S. *email: saenger@chemie.fu-berlin.de* or W.H. *email: hinrichs@mail.uni-greifswald.de*

Received 24 January, 2000; accepted 4 February, 2000.

1. McMurry, L., Petrucci, R.E. & Levy, S.B. *Proc. Natl. Acad. Sci. USA* **77**, 3974–3977 (1980).
2. Yamaguchi, A., Iwasaki-Ohba, Y., Ono, N., Kaneko-Ohdera, M. & Sawai, T. *FEBS Lett.* **282**, 415–418 (1991).
3. Schnappinger, D. & Hillen, W. *Arch. Microbiol.* **165**, 359–369 (1996).
4. Hillen, W. & Berens, C. *Ann. Rev. Microbiol.* **48**, 345–369 (1994).
5. Bertrand, K.P., Postle, K., Wray, Jr., L.V. & Reznikoff, W.S. *Gene* **23**, 149–156 (1983).
6. Eckert, B. & Beck, C.F. *J. Bacteriol.* **171**, 3557–3559 (1989).
7. Kleinschmidt, C., Tovar, K., Hillen, W. & Pörschke, D. *Biochemistry* **27**, 1094–1104 (1988).
8. Lederer, T., Takahashi, M. & Hillen, W. *Anal. Biochemistry* **232**, 190–196 (1995).
9. Gossen, M. *et al*. *Science* **268**, 1766–1769 (1995).
10. Freundlieb, S., Baron, U., Bonin, A.L., Gossen, M. & Bujard, H. *Methods Enzymol.* **283**, 159–173 (1997).
11. Rossi, F.M.V. & Blau, H.M. *Curr. Opin. Biotechnol.* **9**, 451– 456 (1998).
12. Förster, K. *et al*. *Nucleic Acids Res.* **27**, 708–710 (1999).
13. Baron, U. *et al*. *Proc. Natl. Acad. Sci. USA* **96**, 1013–1018 (1999).
14. Hinrichs, W. *et al*. *Science* **264**, 418–420 (1994).
15. Kisker, C., Hinrichs, W., Tovar, K., Hillen, W. & Saenger, W. *J. Mol. Biol*. **247**, 260–280 (1995).
16. Orth, P. *et al*. *J. Mol. Biol.* **279**, 439–447 (1998).
17. Otwinowski, Z. *et al*. *Nature* **335**, 321–329 (1988).
18. Lewis, M. *et al*. *Science* **271**, 1247–1254 (1996).
19. Schumacher, M.A., Choi, K.Y., Lu, F., Zalkin, H. & Brennan, R.G. *Cell* **83**, 147–155 (1995).
20. Steitz, T.A., Ohlendorf, D.H., McKay, D.B., Anderson, W. & Matthews, B.W. *Proc. Natl. Acad. Sci. USA* **79**, 3097–3100 (1982).
21. Heuer, C. & Hillen, W. *J. Mol. Biol.* **202**, 407–415 (1988).
22. Sizemore, C., Wissmann, A., Gülland, U. & Hillen, W. *Nucl. Acids Research* **18**, 2875–2880 (1990).
23. Wissmann, A. *et al*. *EMBO J.* **10**, 4145–4152 (1991).
24. Baumeister, R., Helbl, V. & Hillen, W. *J. Mol. Biol.* **226**, 1257–1270 (1992).
25. Helbl, V., Berens, C. & Hillen, W. *J. Mol. Biol.* **245**, 538–548 (1995).
26. Schwabe, J.W.R. *Curr. Opin. Struct. Biol.* **7**, 126–134 (1997).
27. Harrison, S.C. *Nature* **353**, 715–719 (1991).
28. Müller, G. *et al*. *Nature Struct. Biol.* **2**, 693–703 (1995).
29. Orth, P., Saenger, W. & Hinrichs, W. *Biochemistry* **38**, 191–198 (1999).
30. Degenkolb, J., Takahashi, M., Ellestad, G.A. & Hillen, W. *Antimicrob. Agents Chemother*. **35**, 1591–1595 (1991).
31. Orth, P. *et al*. *J. Mol. Biol*. **285**, 455–461 (1999).
32. Arvidson, D.N., Lu, F., Faber, C., Zalkin, H. & Brennan, R.G. *Nature Struct. Biol.* **5**, 436–441 (1998).
33. Schumacher, M.A., Glasfeld, A., Zalkin, H. & Brennan, R.G. *J. Biol. Chem.* **272**, 22648–22653 (1997).
34. Kercher, M.A., Lu, P. & Lewis, M. *Curr. Opin. Struct. Biol.* **7**, 76–85 (1997).
35. Orth, P., Alings, C., Schnappinger, D., Saenger, W. & Hinrichs, W. *Acta Crystallogr. D* **54**, 99–100 (1998).
36. Otwinowski, Z. & Minor, W. *Methods Enzymol.* **276**, 307–326 (1997).
37. Collaborative Computational Project, Number 4. *Acta Crystallogr. D* **50**, 760–776 (1994).
38. Navaza, J. *Acta Crystallogr. A* **50**, 157–163 (1994).
39. Jones, A.T., Zou, J.-Y., Cowan, S.W. & Kjeldgaard, M. *Acta Crystallogr. A* **47**, 110–119 (1991).
40. Brünger, A.T. *X-PLOR Manual version 3.843* (Yale University Press, New Haven, Connecticut; 1996).
41. Ravishanker, G., Swaminathan, S., Beveridge, D.L., Lavery, R. & Sklenar, H. *J. Biomol. Struct. Dyn*. **6**, 669–699 (1989).
42. Kraulis, P.J. *J. Appl. Crystallogr.* **24**, 946–950 (1991).
43. Merritt, E.A. & Murphy, M.E.P. *Acta Crystallogr*. *D* **50**, 869–873 (1994).